ChemPubSoc Europe

DOI: 10.1002/chem.201800864

CHEMISTRY A European Journal Full Paper

Frustrated Lewis Pairs |*Hot Paper*|

Hydrogenation of Multiple Bonds by Geminal Aminoborane-Based Frustrated Lewis Pairs

Diana Yepes,[a] Pablo Jaque,*[b] and Israel Fernández*[c]

Abstract: The hydrogenation reaction of multiple bonds that is mediated by geminal aminoborane-based frustrated Lewis pairs (FLPs) has been explored by means of density functional theory calculations. It was found that the release of the activated dihydrogen occurred in a concerted, yet highly asynchronous, manner. The physical factors that control the transformation were quantitatively described in detail by using the activation strain model of reactivity in combination with the energy decomposition analysis method. This approach suggested a cooperative double hydrogen-transfer mechanism, which involves the initial migration of the protic (N)H followed by the nucleophilic attack of the (B)H hydride to the carbon atom of the multiple bond. The influence of both the substituents directly attached to the boron atom of the initial FLP and the nature of the multiple bond on the transformation was also investigated.

Introduction

Since the seminal discovery of dihydrogen activation by sterically hindered Lewis acid and Lewis base pairs in 2006 by Stephan and co-workers,[1] the chemistry of the so-called Frustrated Lewis Pairs (FLPs) has experienced a tremendous development. Indeed, in the last decade, an impressive number of studies have focused on different aspects of FLPs, such as the activation of small inert molecules and bonds (e.g., H_2, CO, CO_2, N_2O, etc.), the synthesis of novel, more active FLP systems (even based on transition-metal fragments), and mechanistic investigations.[2]

Among the different applications of FLPs, the hydrogenation of unsaturated organic substrates is arguably one of the most (if not, the most) representative one.[2,3] This is because this approach constitutes a metal-free alternative to traditional transition-metal-mediated hydrogenations, which can also be carried out in a catalytic manner. Nevertheless, the development of enantioselective hydrogenations catalyzed by chiral FLPs still remains a great challenge.[4] Despite the vast number of studies devoted to the FLP-mediated hydrogenation reactions of multiple bonds,[2–5] the physical factors that control the release of the FLP-activated dihydrogen are not yet completely understood.

With this in mind, we recently explored the factors that control the initial step of the process, that is, the dihydrogen activation reaction by a series of geminal aminoborane FLPs.[6] By means of the activation strain model (ASM)[7] of reactivity in combination with the energy decomposition analysis (EDA)[8] method, we gained a detailed quantitative insight into the H_2-activation reaction and proposed an orbital-controlled mechanism. Our findings complemented the previously reported reactivity models, namely, the electron transfer (ET) model, proposed by Pápai and co-workers in analogy with the transition-metal-mediated H_2 activation,[9] and the electric field (EF) model, suggested by Grimme and co-workers.[10] In our approach, the degree of charge transfer cooperativity between the most important donor–acceptor orbital interactions, that is, LP(N)→σ*(H_2) and σ(H_2)→p_π(B), along the reaction coordinate constitutes a suitable indicator of the reaction barrier.

Given the good performance of the combined ASM–EDA methodology on the chemistry of FLPs, we decided to complete the study of the transformation by considering the subsequent dihydrogen release, which leads to the reduction of multiple bonds. To this end, we focused on the processes that involves the most representative FLPs (i.e., those that have feasible H_2 activation barriers) and different multiple bonds, which includes either polar (O=C, N=C) or nonpolar (C=C, C≡C) bonds (Scheme 1). The selected transformations were chosen to quantitatively assess the influence of both the substituents at the FLP and the nature of the multiple bond on the transformation. Even though it has been found that related geminal aminoborane species ($R_2NCH_2BAr_2$) form head-to-tail dimers and oligomers under certain conditions,[11] the studied systems can still be considered as model compounds of more realistic geminal B/N[12] or B/P[13] FLPs.

[a] *Dr. D. Yepes*
Departamento de Ciencias Químicas, Facultad de Ciencias Exactas
Universidad Andres Bello, Av. República 275, Santiago (Chile)

[b] *Dr. P. Jaque*
Departamento de Química Orgánica y Fisicoquímica
Facultad de Ciencias Químicas y Farmacéuticas
Universidad de Chile, Sergio Livingstone 1007, Santiago (Chile)
E-mail: pablo.jaque@ciq.uchile.cl

[c] *Prof. Dr. I. Fernández*
Departamento de Química Orgánica I and Centro de Innovación en Química Avanzada (ORFEO-CINQA), Facultad de Ciencias Químicas
Universidad Complutense de Madrid, 28040 Madrid (Spain)
E-mail: israel@quim.ucm.es

Supporting information and the ORCID number(s) for the author(s) of this article can be found under https://doi.org/10.1002/chem.201800864.

© 2018 Wiley-VCH Verlag GmbH & Co. KGaA, Weinheim

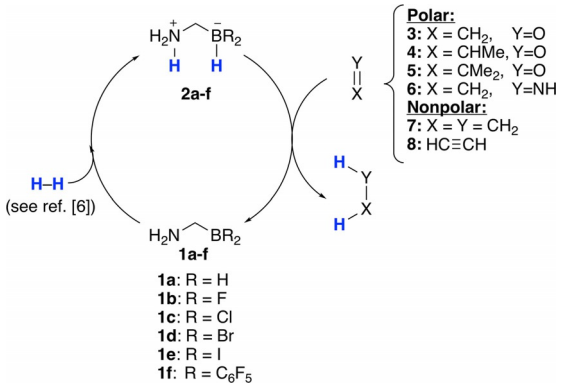

Scheme 1. Hydrogenation reactions mediated by α,α-disubstituted geminal aminoborane-based FLPs considered in this study.

Theoretical Methods and Computational Details

To enable a direct comparison, we have used the same level of theory as that used in our previous study on the FLP–dihydrogen activation.[6] Therefore, geometry optimizations of the molecules were performed without symmetry constraints by using the Gaussian 09 suite of programs[14] and employing the meta-hybrid M06-2X exchange–correlation functional[15] combined with the triple-ζ quality def2-TZVPP basis set.[16] Reactants and products were characterized by frequency calculations and have positive definite Hessian matrices. Transition states (TSs) showed only one negative eigenvalue in their diagonalized force constant matrices, and their associated eigenvectors were confirmed to correspond to the motion along the reaction coordinate under consideration by using the intrinsic reaction coordinate (IRC) method.[17] In addition, the vibrational calculation provided the thermal Gibbs energy corrections by using the gas ideal rigid rotor/harmonic oscillator approximation. Solvent effects were taken into account with the polarizable continuum model (PCM)[18] by using the gas-phase-optimized geometries at the same level. This level is denoted PCM(solvent)/M06-2X/def2-TZVPP//M06-2X/def2-TZVPP. Energy decomposition analyses were carried out by using the ADF.2014 program[19] at the dispersion-corrected BP86[20]-D3[21] level of theory in conjunction with the triple-ζ quality TZ2P basis set[22] on the geometries optimized at the M06-2X/def2-TZVPP level. Core electrons were described in a frozen-core approximation, and the scalar relativistic effects were accounted for by using the zeroth-order regular approximation (ZORA).[23] Therefore, this level is denoted ZORA-BP86-D3/TZ2P//M06-2X/def2-TZVPP.

Activation strain model of reactivity

The ASM of reactivity method is a systematic development of the EDA method (see below). This method, which is also known as the distortion/interaction model,[24] is a fragment approach to understanding chemical reactions in which the height of reaction barriers is described and understood in terms of the original reactants.[7] Within this approach, the potential energy surface $\Delta E(\zeta)$ [Eq. (1)], along the reaction coordinate ζ, is made up of two main contributions: the strain $\Delta E_{strain}(\zeta)$ associated with deforming the individual reactants and the actual interaction $\Delta E_{int}(\zeta)$ between these increasingly deformed reactants:

$$\Delta E(\zeta) = \Delta E_{strain}(\zeta) + \Delta E_{int}(\zeta) \quad (1)$$

The strain $\Delta E_{strain}(\zeta)$ depends on both the rigidity of the reactants and the reaction pathway under consideration, and the interaction $\Delta E_{int}(\zeta)$ between the reactants depends on their electronic structure and on their mutual orientation as they approach each other. The interplay between $\Delta E_{strain}(\zeta)$ and $\Delta E_{int}(\zeta)$ determines where the barrier arises, namely, at the point that satisfies $d\Delta E_{strain}(\zeta)/d\zeta = -d\Delta E_{int}(\zeta)/d\zeta$. This approach has enormously contributed to our current understanding of different fundamental transformations in organic[25] and organometallic chemistry.[26] For further details of the theoretical background and different applications of the ASM method, we refer readers to recently published review articles.[7]

Herein, for consistency reasons, the reaction coordinate was defined as the projection of the IRC onto the forming BH···C distance. This reaction coordinate ζ undergoes a well-defined change over the course of the reaction from the initial reactant complexes to the equilibrium BH···C distance in the corresponding transition states.

Energy decomposition analysis

The interaction $\Delta E_{int}(\zeta)$ between the strained reactants can be further partitioned into chemically meaningful contributions by means of the EDA method.[8,27] Thus, $\Delta E_{int}(\zeta)$ is composed of the following terms [Eq. (2)] along the reaction coordinate:

$$\Delta E_{int}(\zeta) = \Delta V_{elstat}(\zeta) + \Delta E_{Pauli}(\zeta) + \Delta E_{orb}(\zeta) + \Delta E_{disp}(\zeta) \quad (2)$$

The term ΔV_{elstat} corresponds to the classical electrostatic interaction between the unperturbed charge distributions of the deformed reactants and is usually attractive. The Pauli repulsion ΔE_{Pauli} comprises the destabilizing interactions between occupied orbitals and is responsible for any steric repulsion. The orbital interaction ΔE_{orb} accounts for charge transfer (interaction between occupied orbitals on one moiety with unoccupied orbitals on the other, which includes HOMO–LUMO interactions) and polarization (empty–occupied orbital mixing on one fragment owing to the presence of another fragment). Finally, the ΔE_{disp} term takes into account the interactions that are due to dispersion forces. Moreover, the NOCV (natural orbital for chemical valence)[28] extension of the EDA method has been used to further partition the ΔE_{orb} term. The EDA–NOCV approach provides the pairwise energy contributions for each pair of interacting orbitals to the total bond energy.

Results and Discussion

Figure 1 shows the computed reaction profile for a representative hydrogenation reaction that involves zwitterion **2f** (R=

© 2018 Wiley-VCH Verlag GmbH & Co. KGaA, Weinheim

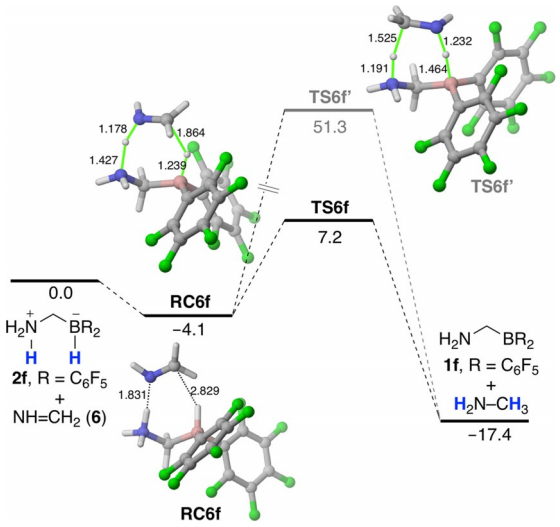

Figure 1. Computed reaction profile for the hydrogenation reaction between zwitterionic species **2 f** and methanimine (**6**). Relative free energies (ΔG, computed at 298 K) and bond lengths are given in kcal mol^{-1} and Å, respectively. All data have been computed at the M06-2X/def2-TZVPP level.

C_6F_5) and methanimine (**6**). The reduction of substrate **6** by **2 f** proceeds in a concerted manner via an initial reactant complex **RC6 f**; this is transformed into the corresponding reaction products through the transition state **TS6 f** to give methylamine ($H_2N–CH_3$) and FLP **1 f**. This saddle point is associated with the concerted (yet asynchronous) migration of both hydrogen atoms from zwitterion **2 f** to imine **6**, which involves the nucleophilic attack of the B–H hydride species onto the electrophilic carbon atom of imine **6** and the N–H proton migration onto the nitrogen atom of the imine. The transformation can be formally viewed as a double group transfer reaction (DGTR),[29] which resembles textbook reactions, such as the diimide reduction of double or triple bonds,[30] the Meerwein–Ponndorf–Verley reduction (MPV) of carbonyl groups,[31] some type II dyotropic reactions that are characterized by the intramolecular transfer of the two groups (generally hydrogen atoms),[32] and even the transition-metal-catalyzed (Noyori-type) hydrogenation reaction of polar bonds.[33] The computed low activation barrier ($\Delta G^{\neq} = 11.3$ kcal mol^{-1}) and exergonic reaction energy ($\Delta G_R = -17.4$ kcal mol^{-1}) are fully compatible with a process that occurs at room temperature.[2,3,34] Alternatively, the reaction products can also be formed through transition state **TS6 f"**, in which the B–H hydride species migrates to the nucleophilic nitrogen atom of the imine instead of to the electrophilic carbon center. Not surprisingly, the computed activation barrier for this counterintuitive reaction is rather high ($\Delta G^{\neq} = 55.4$ kcal mol^{-1}), which renders this alternative pathway kinetically unfeasible. Moreover, similar reaction profiles were computed for the more realistic geminal B/N FLP 1-[bis(pentafluorophenyl)boryl]-3,5-di-methyl-1*H*-pyrazole[12] and B/P FLP $Me_2PCH_2BPh_2$,[13] which provides further support for the model compounds that are considered herein (see the Supporting Information, Figure S1).

Similar reaction profiles to that discussed above for the reaction **2 f**+**6**→**1 f**+$H_2N–CH_3$ have been computed for the rest of the considered transformations. For instance, the optimized geometries of all the transition states associated with the hydrogenation of methanimine (**TS6 a**–**f**) or formaldehyde (**TS3 a**–**f**) clearly confirm that the process occurs in a concerted manner, regardless of the substituent attached to the boron atom of zwitterions **2** (Figure 2).[35] Closer inspection of these

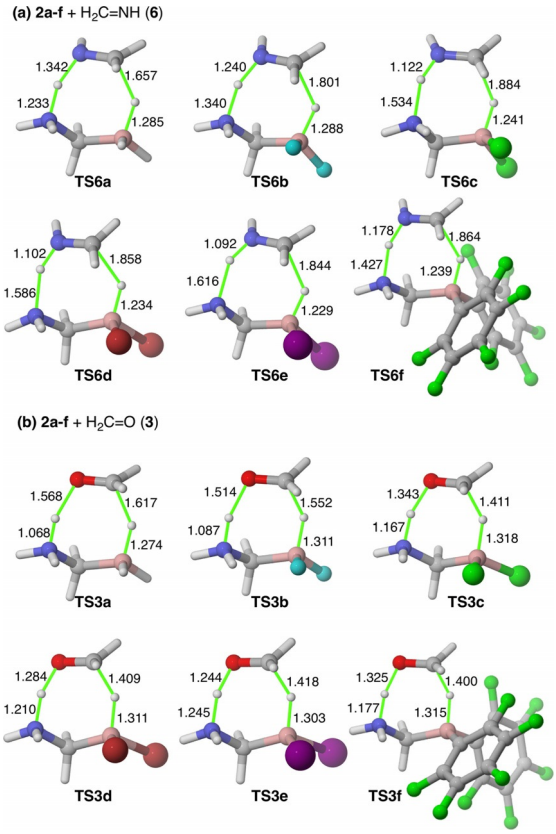

Figure 2. Fully optimized geometries (M06-2X/def2-TZVPP level) of the transition states involved in the hydrogenation of a) methanimine and b) formaldehyde by zwitterionic species **2 a**–**f**. Bond lengths are given in Å.

saddle points indicates that, in all cases, the formation of the new C–H bond is slower than the formation of the N–H bond. Interestingly, according to the computed barrier and reaction energies (Table 1; for the energies computed for the alternative noncompetitive pathways, see the Supporting Information, Table S1), it can be observed that shorter N–H bond forming (or longer N–H bond breaking) distances are associated with higher reaction barriers. In particular, lower reaction barriers are found for those hydrogenation processes that involve highly electronegative substituents (e.g., F) or strongly electron-withdrawing groups (e.g., C_6F_5) attached to the boron atom (for instance, the computed activation barrier increased from 9.9 to 14.7 kcal mol^{-1} for R = F and I, respectively). Indeed, a good linear relationship was found when the N–H bond breaking distance in the transition states **TS6 a**–**f** (or **TS3 a**–**f**, for the hydrogenation of O=CH_2) were plotted against the corresponding computed activation barriers (correlation coefficients of 0.98 and 0.96, respectively, Figure 3). Therefore,

© 2018 Wiley-VCH Verlag GmbH & Co. KGaA, Weinheim

Table 1. Computed activation and reaction energies plus ZPVE corrections (free energies, computed at 298.15 K, are given within parentheses) for the hydrogenation reactions of substrates **3**–**8** by the zwitterionic species **2a**–**f**. All data [kcal mol^{-1}] were computed at the M06-2X/def2-TZVPP level.

	$\Delta E^{\neq}$ ($\Delta G^{\neq}$)[a]						ΔE_R (ΔG_R)[b]					
	3	4	5	6	7	8	3	4	5	6	7	8
2a	0.9	4.9	7.1	6.9	20.9	21.7	−21.8	−16.1	−12.5	−25.9	−32.1	−39.9
	(2.3)	(5.6)	(9.3)	(8.9)	(23.9)	(23.6)	(−22.5)	(−16.3)	(−11.9)	(−26.5)	(−32.7)	(−44.6)
2b	3.4	6.4	9.0	8.2	22.3	23.2	−36.1	−30.3	−26.7	−40.2	−46.4	−54.2
	(5.4)	(8.2)	(11.3)	(9.9)	(25.4)	(25.2)	(−36.8)	(−30.7)	(−26.3)	(−40.9)	(−47.0)	(−59.0)
2c	7.8	10.6	13.0	11.5	26.9	26.2	−18.4	−12.7	−9.1	−22.5	−28.7	−36.5
	(9.7)	(13.6)	(15.8)	(13.2)	(30.5)	(28.6)	(−19.2)	(−13.1)	(−8.7)	(−23.3)	(−29.4)	(−41.3)
2d	9.8	12.4	15.1	12.6	28.5	27.4	−12.3	−6.6	−3.0	−16.4	−22.6	−30.4
	(11.8)	(14.8)	(17.0)	(14.3)	(31.5)	(29.9)	(−13.1)	(−6.9)	(−2.5)	(−17.1)	(−23.3)	(−35.2)
2e	11.2	13.3	15.6	12.9	29.4	28.0	−7.4	−1.7	1.9	−11.5	−17.7	−25.5
	(13.3)	(15.9)	(18.5)	(14.7)	(32.3)	(30.4)	(−8.2)	(−2.1)	(2.4)	(−12.3)	(−18.4)	(−30.3)
2f	7.0	9.1	13.8	10.2	26.6	25.6	−13.0	−7.3	−3.7	−17.2	−23.3	−31.1
	(9.1)	(11.0)	(16.9)	(11.3)	(29.7)	(27.6)	(−13.3)	(−7.2)	(−2.8)	(−17.4)	(−23.5)	(−35.4)

[a] Activation energy: $\Delta E^{\neq} = E(\mathbf{TS}) - E(\mathbf{RC})$. [b] Reaction energy: $\Delta E_R = E$(reduced **3**–**8**)+E(**1a**–**f**)−E(**3**–**8**)−E(**2a**–**f**).

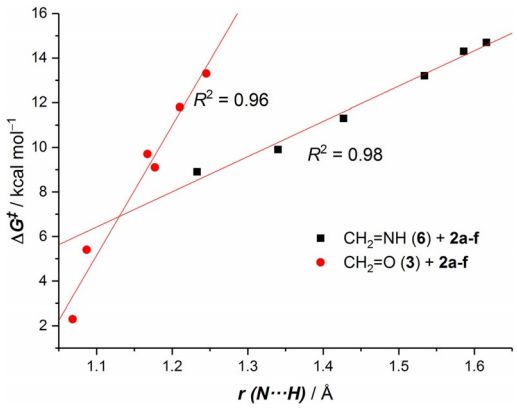

Figure 3. Plot of the computed activation barriers ($\Delta G^{\neq}$) against the N–H bond breaking distance in the transition states **TS6a**–**f** (black squares) and **TS3a**–**f** (red circles). All data were computed at the M06-2X/def2-TZVPP level.

late transition states (i.e., having less electronegative groups attached to the boron atom) are associated with higher activation barriers than early transition states, which agrees with the Hammond–Leffer postulate.[36]

To check the effect of the solvent in these hydrogenation reactions, single-point-energy refinements were carried out at the PCM-M06-2X/def2-TZVPP method. Initially, toluene was chosen as the solvent (Table 2). As a result, the barrier energies in solution were only slightly higher (2–3 kcal mol^{-1}) than those computed at the gas phase, whereas the reaction energies become systematically less exergonic (ca. 7 kcal mol^{-1}) owing to the loss of the zwitterionic character of species **2a**–**f** upon dihydrogen transfer. Not surprisingly, this effect was much more significant when a polar solvent was used, such as dimethyl sulfoxide, which was confirmed by our calculations on selected dehydrogenation reactions (see the Supporting Information, Table S2).

Different reactivity trends can be observed when inspecting the data gathered in Table 1. On the one hand and as commented above, the hydrogenation of a substrate with highly electronegative groups attached to the boron atom of zwitterions **2** leads to lower reaction barriers ($\Delta G^{\neq}$ increased in the

Table 2. Computed activation and reaction energies in toluene plus ZPVE corrections (free energies, computed at 298.15 K, are given within parentheses) for the hydrogenation reactions of substrates **3**–**8** by the zwitterionic species **2a**–**f**. All data [kcal mol^{-1}] were computed at the PCM(toluene)/M06-2X/def2-TZVPP//M06-2X/def2-TZVPP level.

	$\Delta E^{\neq}$ ($\Delta G^{\neq}$)[a]						ΔE_R (ΔG_R)[b]					
	3	4	5	6	7	8	3	4	5	6	7	8
2a	2.3	6.8	9.2	9.8	24.9	24.6	−14.8	−8.7	−5.0	−18.7	−24.9	−32.3
	(3.7)	(7.5)	(11.4)	(11.9)	(27.9)	(26.5)	(−15.4)	(−9.0)	(−4.4)	(−19.3)	(−25.4)	(−37.0)
2b	5.1	8.3	11.0	10.3	26.1	25.9	−28.4	−22.4	−18.7	−32.3	−38.5	−46.0
	(7.1)	(10.1)	(13.3)	(12.0)	(29.2)	(27.9)	(−29.2)	(−22.8)	(−18.2)	(−33.0)	(−39.2)	(−50.8)
2c	10.6	13.8	16.1	12.3	34.7	29.6	−10.6	−4.6	−0.8	−14.5	−20.7	−28.2
	(12.5)	(16.7)	(18.8)	(14.0)	(30.5)	(32.0)	(−11.4)	(−5.0)	(−0.4)	(−15.3)	(−21.4)	(−33.0)
2d	12.8	15.6	17.9	13.2	35.7	31.0	−4.7	1.4	5.1	−8.5	−14.7	−22.2
	(14.8)	(18.1)	(19.8)	(14.9)	(31.5)	(33.5)	(−5.4)	(1.0)	(5.6)	(−9.2)	(−15.4)	(−27.0)
2e	14.3	16.6	18.8	13.5	36.3	31.5	−0.1	6.0	9.7	−4.0	−10.2	−17.6
	(16.4)	(19.2)	(21.7)	(15.2)	(32.3)	(33.9)	(−0.9)	(5.6)	(10.2)	(−4.7)	(−10.9)	(−22.4)
2f	8.9	11.2	15.9	11.5	33.2	28.2	−7.2	−1.1	2.6	−11.1	−17.3	−24.7
	(11.1)	(13.1)	(19.0)	(12.6)	(29.7)	(30.2)	(−7.5)	(−1.0)	(3.6)	(−11.3)	(−17.5)	(−29.0)

[a] Activation energy: $\Delta E^{\neq} = E(\mathbf{TS}) - E(\mathbf{RC})$. [b] Reaction energy: $\Delta E_R = E$(reduced **3**–**8**)+E(**1a**–**f**)−E(**3**–**8**)−E(**2a**–**f**).

© 2018 Wiley-VCH Verlag GmbH & Co. KGaA, Weinheim

order F < Cl < Br < I). In this sense, the incorporation of a C_6F_5 group, which is widely used in FLP chemistry, results in a behavior between that of substrates with F and Cl substituents. Strikingly, this reactivity trend is opposite to that found for the dihydrogen activation by using the same FLPs (the corresponding barriers increased in the order I < Br < Cl < F),[6] which highlights the markedly different nature of both steps of the FLP-mediated hydrogenation reaction. Therefore, it can be concluded that good substituents for the dihydrogen activation are not necessarily also good substituents for the subsequent hydrogen release. For instance, the activation barrier computed for the H_2 activation by $H_2NCH_2B(OMe)_2$ (**1g**) was rather high ($\Delta G^{\ddagger}$ = 34.9 kcal mol^{-1}),[6] whereas the subsequent hydrogenation of O=CH_2 had an activation barrier of only 2.8 kcal mol^{-1} (which is even lower than that computed for the analogous reaction that involves the fluorine derivative **2b**, $\Delta G^{\ddagger}$ = 5.4 kcal mol^{-1}, Table 1). We will revisit this issue in conjunction with the activation strain analyses, discussed below.

On the other hand, for a given zwitterion **2a–f**, it was systematically observed that the hydrogenation of methanimine (**6**) was kinetically more difficult than that of formaldehyde (**3**), which is consistent with the lower electrophilicity of the carbon atom of substrate **6**. In addition, the attachment of methyl substituents to the carbon atom in substrate **3** led to higher barriers ($\Delta G^{\ddagger}$ increased in the order **3** < **4** < **5**), which suggests that the steric hindrance at that carbon atom hampers the nucleophilic B–H hydride attack. Furthermore, it was found that the hydrogenation of nonpolar bonds (reactions that involve substrates **7** and **8**) proceeded with much higher reaction barriers ($\Delta G^{\ddagger}$ = 23–32 kcal mol^{-1}) than the analogous processes that involve polar bonds. This was ascribed to the occurrence of a significant noncovalent interaction in the initial reactant complexes, that is, a hydrogen bond is established between the protic N–H moiety of zwitterion **2** and the lone pair of the heteroatom of substrates **3**–**6**, which brings both reactants into closer proximity and makes the interaction between them much stronger. This stabilizing interaction, which is not present in the processes that involve substrates **7** and **8**, can be easily visualized by means of the noncovalent interaction (NCI) method.[37] As is illustrated in Figure 4, reactant complexes **RC3b** and **RC6b** exhibited a strong noncovalent interaction (blue region) between the N–H moiety of the zwitterion and the heteroatom of the substrate, which clearly confirms the occurrence of the hydrogen bond. In contrast, the analogous species that is involved in the hydrogenation of ethylene, **RC7b**, only exhibited a weak interaction (green surface), which is the result of a N–H···π interaction.

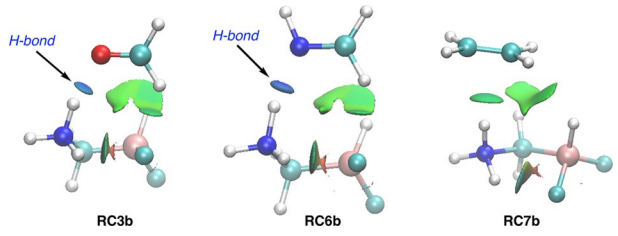

Figure 4. NCI surfaces computed for reactant complexes **RC3b**, **RC6b**, and **RC7b**. Blue and green areas indicate strong and weak noncovalent interactions, respectively.

To further confirm the crucial role of this hydrogen bond on the interaction between the reactants, we applied the ASM of reactivity. Figure 5 shows the computed activation strain diagrams (ASDs) for the hydrogenation reactions of methanimine (**6**) and ethylene (**7**) by zwitterion **2b** (R = F) from the corresponding reactant complexes to the respective transition states. Both processes exhibited quite similar ASDs such that the interaction energy between the deformed reactants, which is measured by the ΔE_{int} term, remained constant or became slightly destabilizing at the beginning of the reaction and inverted at the proximity of the transition state region, at which point it became increasingly stabilizing. The same behavior was found in strongly related DGTRs[38] and other pericyclic reactions.[7,39] Despite this, the process that involved the polar N=C bond clearly exhibited a much stronger interaction between the reactants, not only at the beginning of the process (when the NH···N hydrogen bond is established) but also, as anticipated, along the entire reaction coordinate. This stronger interaction was even able to compensate for the more destabilizing deformation energy (measured by the ΔE_{strain}) that was computed for the hydrogenation of imine **6** compared with the process that involves substrate **7**. As a result, the hydrogenation of imine **6** (and of similar systems that have polar C=X bonds) occurred with a much lower activation barrier than that of the analogous process that involves the nonpolar C=C (or C≡C) bond.

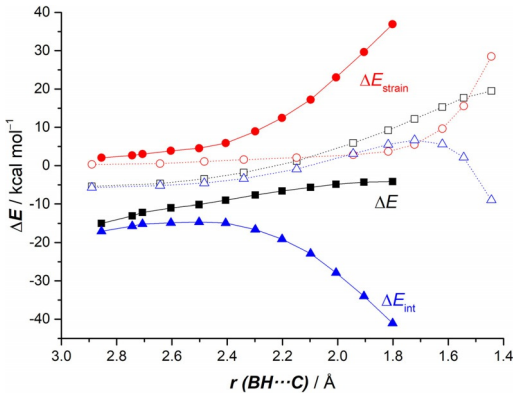

Figure 5. Comparative activation strain diagrams of the hydrogenation reactions of methanimine (**6**, solid lines) and ethylene (**7**, dotted lines) mediated by zwitterion **2b** along the reaction coordinate projected onto the BH···C bond forming distance. All data were computed at M06-2X/def2-TZVPP level and referenced to the isolated reactants.

We also applied the ASM method to understand the influence that the substituent that is attached to the boron atom has on the transformation. To this end, the hydrogenation reactions of methanimine mediated by zwitterions **2b** and **e** (R = F and I, respectively) were compared (the former process occurred with a slightly lower activation barrier, see above). The corresponding ASDs depicted in Figure 6 indicate that the differences between the processes occur mainly at the transition

© 2018 Wiley-VCH Verlag GmbH & Co. KGaA, Weinheim

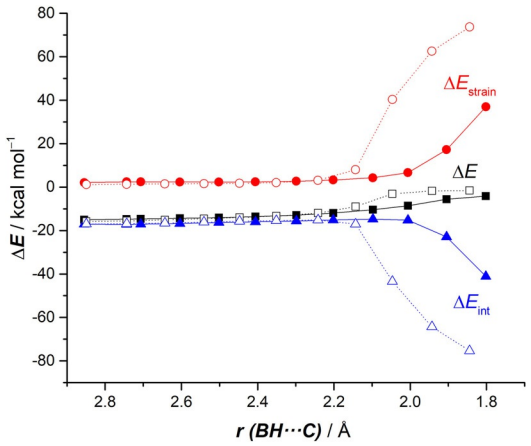

Figure 6. Comparative activation strain diagrams of the hydrogenation reactions of methanimine (**6**) mediated by zwitterions **2b** (solid lines) and **e** (dotted lines) along the reaction coordinate projected onto the BH···C bond forming distance. All data were computed at M06-2X/def2-TZVPP level and referenced to the isolated reactants.

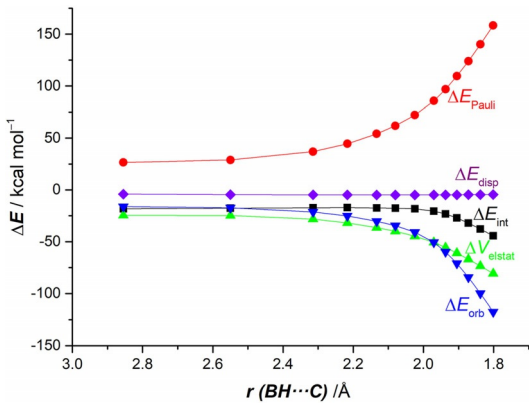

Figure 7. Energy decomposition analysis of the hydrogenation of methanimine (**6**) by zwitterionic species **2b** (R = F) along the reaction coordinate projected onto the BH···C bond forming distance (in Å). All data were computed at ZORA-BP86-D3/TZ2P//M06-2X/def2-TZVPP level.

state region, that is, the part of the reaction coordinate at which the BH···C bond formation occurs. In the case of the reaction with substrate **2e**, the interaction energy between the fragments increased significantly compared with the process that involved substrate **2b**. However, simultaneously, the strain term became highly destabilizing, which can offset the stabilizing contribution of ΔE_{int}. For this reason, the barrier computed for the **2e+6** reaction was slightly higher than that computed for the hydrogenation with substrate **2b**. In addition, these ASDs, which are projected onto the BH···C bond forming distance, suggest that, at the beginning of the process, only the NH···N bond formation occurred and that this proton migration was similar for both systems. Indeed, the corresponding ASDs projected onto the NH···N bond forming distance are nearly identical for both reactions (see the Supporting Information, Figure S2). This finding further supports the highly asynchronous nature of this particular type of DGTR.

We finally used the EDA method to gain further quantitative insight into the different contributions to the total interaction energy between the fragments along the reaction coordinate. Figure 7 graphically shows the variation of the EDA terms that were computed for the hydrogenation of methanimine by zwitterion **2b** (R = F) from the initial reactant complex **RC6b** to the corresponding transition state **TS6b**, which was considered to be a representative example of the hydrogenation reactions in this study. It became clear that the interaction from dispersion forces (ΔE_{disp}) remained constant along the entire transformation; therefore, it does not control the increase of the ΔE_{int} at the transition state region. In contrast, both the orbital (ΔE_{orb}) and electrostatic (ΔV_{elstat}) attractions, the latter in a lesser extent, became increasingly more stabilizing, particularly at the transition state region, and could compensate for the destabilization from the repulsive ΔE_{Pauli} term. It is notable that the electrostatic term became the major contributor to the total interaction energy between the reactants at the early stage of the process, which is dominated by the $^{+}$NH···N interaction. In contrast, as one approaches the transition state, the BH···C bond formation occurs, and this makes the orbital term increasingly more stabilizing; as a result, this constitutes the major contributor to the total interaction energy (for instance, at the transition state, ΔE_{orb} accounts for ≈60% of the total attractive interactions between the reactants).

The crucial role of the orbital interactions between the deformed reactants along the reaction coordinate deserved further analysis. Therefore, we decided to apply the energy decomposition analysis combined with the natural orbitals for chemical valence (EDA-NOCV)[28] method to not only identify but also quantify the main orbital interactions that occur between the reactants along the transformation. According to the EDA-NOCV method, two main pairwise orbital interactions dominate the ΔE_{orb} term: the LP(*N*-methanimine)→σ*(N–H-**2b**) and the σ(B–H-**2b**)→π*(N=CH_2-methanimine) interactions. Snapshots of the respective NOCV deformation densities (denoted as $\Delta\rho_1$ and $\Delta\rho_2$) associated with these interactions at three key points (reactant complex, midpoint, and TS) along the reaction coordinate are shown in Figure 8. At the beginning of the process, only the LP(*N*-methanimine)→σ*(N–H-**2b**) interaction takes place as a consequence of the occurrence of the intermolecular NH···N hydrogen bond, discussed above. According to computed values of the associated NOCV-orbital energies ($\Delta E(\rho)$), this charge transfer process was continuously reinforced as the reaction progressed ($\Delta E(\rho_1)$ increased from −11.0 kcal mol^{-1} in the reactant complex to −33.5 kcal mol^{-1} in the transition state). However, this orbital interaction did not become the major contributor to the total orbital attractions between the deformed reactants at the proximities of the transition state region. Instead, the σ(B–H-**2b**)→π*(N=CH_2-methanimine) interaction, which is negligible at the beginning of the process, became increasingly more significant (for instance, $\Delta E(\rho_2)$ is ca. twice as strong as $\Delta E(\rho_1)$ at the transition state), which firmly confirms the high asynchronicity of the hydrogen transfers in these FLP-mediated hydrogenation reactions.

A clear picture of the mechanism of the dihydrogen release by zwitterions **2** emerged from our ASM-EDA(NOCV) study: the reaction starts with the formation of a strong NH···N hydrogen bond, which brings both reactants into close enough proximity

© 2018 Wiley-VCH Verlag GmbH & Co. KGaA, Weinheim

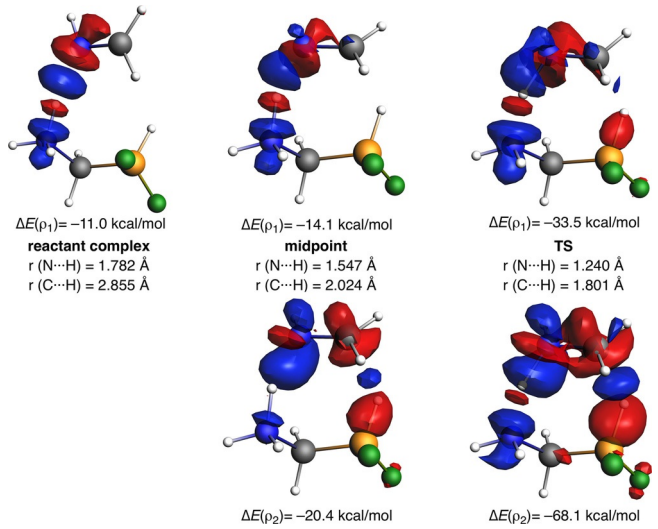

Figure 8. Contour plots of NOCV deformation densities $\Delta\rho$ and associated energies $\Delta E(\rho)$ (in kcal mol^{-1}) for the main orbital interactions between methanimine (**6**) and zwitterion **2b** (R = F) at three key points (reactant complex, midpoint, and TS) along the reaction coordinate. Charge flows from red to blue. All data were computed at ZORA-BP86-D3/TZ2P//M06-2X/def2-TZVPP level.

to interact with each other. Then, the migration of the protic H(–N) hydrogen atom of the zwitterion to the nitrogen atom of the imine begins, whereas the hydride H(–B) remains mainly unaltered. As the new (H_2C=)N···H bond starts to form, it induces a strong polarization in the C=N double bond of the imine, which allows the subsequent nucleophilic addition of the hydride. This cooperative mechanism strongly resembles the typical hydride nucleophilic addition to multiple bonds that is catalyzed by Lewis acids. For the hydrogenation reactions mediated by geminal N/B FLPs, considered herein, the process occurs in a concerted (yet asynchronous) manner, which is reflected in the rather low activation barriers computed for these transformations.

Conclusion

From the computational study reported herein, the following conclusions can be drawn: 1) The release of activated dihydrogen by geminal N/B FLPs that leads to the reduction of unsaturated bonds occurs in a concerted, yet highly asynchronous, manner; this resembles typical textbook double group transfer reactions, like the diimide reduction of double and triple bonds. 2) The hydrogenation of polar multiple bonds (C=O, C=N) is much easier, from a kinetic point of view, than the analogous process that involves nonpolar bonds (C=C, C≡C). 3) The latter is mainly due to the occurrence of an initial hydrogen bond between the NH moiety of the zwitterion and the heteroatom of the substrate, which significantly increases the interaction between the reactants, not only at the beginning of the process but also along the entire reaction coordinate. This key interaction is not present in the reaction of nonpolar bonds, and as a result, the interaction between the reactants is markedly reduced, which is translated into much higher activation barriers for these species. 4) Although the computed activation barrier differences are subtle, it seems that highly electronegative groups attached to the boron atom of the zwitterions lead to lower reaction barriers. This reactivity trend is opposite to that found for the initial dihydrogen activation step. 5) According to the EDA-NOCV method, two main orbital interactions dominate the total orbital attractions between the reactants throughout this process, namely, the LP(heteroatom)→σ*(N–H-**2**) interaction and the σ(B–H-**2**)→π*(X=CH_2) interaction. The former dominates at the early stages of the transformation, whereas the latter becomes the major contributor to the total ΔE_{orb} term in the transition state region. 6) Finally, this particular hydrogenation reaction can be viewed as a cooperative double hydrogen migration reaction, in which the initial migration of the protic (N)H atom induces a polarization of the multiple bond and allows the subsequent (B)H hydride transfer.

Acknowledgements

The authors acknowledge the financial support of the Spanish MINECO-FEDER (Grants CTQ2016-81797-REDC and CTQ2016-78205-P to I.F.) and FONDECYT (Grant No. 1140340 to P.J.), the FONDECYT (Postdoctorado No. 3150249 to D.Y.).

Conflict of interest

The authors declare no conflict of interest.

Keywords: density functional calculations · frustrated Lewis pairs · hydrogenation · multiple bonds · reaction mechanisms

[1] G. C. Welch, R. R. San Juan, J. D. Masuda, D. W. Stephan, *Science* **2006**, *314*, 1124.

[2] For leading reviews, see: a) D. W. Stephan, G. Erker, *Angew. Chem. Int. Ed.* **2010**, *49*, 46; *Angew. Chem.* **2010**, *122*, 50; b) G. Erker, *Pure Appl. Chem.* **2012**, *84*, 2203; c) D. W. Stephan, G. Erker, *Frustrated Lewis Pairs I, Topics in Current Chemistry, Vol. 332*, Springer, **2013**; d) D. W. Stephan, G. Erker, *Chem. Sci.* **2014**, *5*, 2625; e) D. W. Stephan, *J. Am. Chem. Soc.* **2015**, *137*, 10018; f) D. W. Stephan, G. Erker, *Angew. Chem. Int. Ed.* **2015**, *54*, 6400; *Angew. Chem.* **2015**, *127*, 6498; g) D. W. Stephan, *Acc. Chem. Res.* **2015**, *48*, 306; h) D. W. Stephan, *Science* **2016**, *354*, aaf7229; i) S. Arndt, M. Rudolph, A. S. K. Hashmi, *Gold Bull.* **2017**, *50*, 267.

[3] See also: a) T. Soós, *Pure Appl. Chem.* **2011**, *83*, 667; b) D. W. Stephan, S. Greenberg, T. W. Graham, P. Chase, J. J. Hastie, S. J. Geier, J. M. Farrell, C. C. Brown, Z. M. Heiden, G. C. Welch, M. Ullrich, *Inorg. Chem.* **2011**, *50*, 12338; c) D. W. Stephan, *Org. Biomol. Chem.* **2012**, *10*, 5740; d) J. Paradies, *Synlett* **2013**, *24*, 777; e) J. Paradies, *Angew. Chem. Int. Ed.* **2014**, *53*, 3552; *Angew. Chem.* **2014**, *126*, 3624.

[4] For a recent review, see: W. Meng, X. Feng, H. Du, *Acc. Chem. Res.* **2018**, *51*, 191.

[5] Selected examples: a) L. Greb, S. Tussing, B. Schirmer, P. Ona-Burgos, K. Kaupmees, M. Lokov, I. Leito, S. Grimme, J. Paradies, *Chem. Sci.* **2013**, *4*, 2788; b) L. J. Hounjet, C. Bannwarth, C. N. Garon, C. B. Caputo, S. Grimme, D. W. Stephan, *Angew. Chem. Int. Ed.* **2013**, *52*, 7492; *Angew. Chem.* **2013**, *125*, 7640; c) Y. Wang, W. Chen, Z. Lu, Z. H. Li, H. Wang, *Angew. Chem. Int. Ed.* **2013**, *52*, 7496; *Angew. Chem.* **2013**, *125*, 7644; d) Y. Liu, H. Du, *J. Am. Chem. Soc.* **2013**, *135*, 12968; e) K. Chernichenko, Á. Madarász, I. Pápai, M. Nieger, M. Leskelä, T. Repo, *Nat. Chem.* **2013**, *5*, 718.

[6] D. Yepes, P. Jaque, I. Fernández, *Chem. Eur. J.* **2016**, *22*, 18801.

© 2018 Wiley-VCH Verlag GmbH & Co. KGaA, Weinheim

[7] For reviews on the ASM method, see: a) W.-J. van Zeist, F. M. Bickelhaupt, *Org. Biomol. Chem.* **2010**, *8*, 3118; b) I. Fernández, F. M. Bickelhaupt, *Chem. Soc. Rev.* **2014**, *43*, 4953; c) L. P. Wolters, F. M. Bickelhaupt, *WIREs Comput. Mol. Sci.* **2015**, *5*, 324; d) F. M. Bickelhaupt, K. N. Houk, *Angew. Chem. Int. Ed.* **2017**, *56*, 10070; *Angew. Chem.* **2017**, *129*, 10204. See also, e) I. Fernández in *Discovering the Future of Molecular Sciences* (Ed.: B. Pignataro), Wiley-VCH, Weinheim, **2014**, pp. 165 – 187.

[8] For reviews on the EDA method, see: a) F. M. Bickelhaupt, E. J. Baerends, in *Reviews in Computational Chemistry, Vol. 15* (Eds.: K. B. Lipkowitz, D. B. Boyd), Wiley-VCH, New York, **2000**, pp. 1 – 86; b) M. von Hopffgarten, G. Frenking, *WIREs Comput. Mol. Sci.* **2012**, *2*, 43; c) L. Zhao, M. von Hopffgarten, D. M. Andrada, G. Frenking, *WIREs Comput. Mol. Sci.* **2017**, *8*, e1345.

[9] a) T. A. Rokob, A. Hamza, I. Pápai, *J. Am. Chem. Soc.* **2009**, *131*, 10701; b) T. A. Rokob, I. Bakó, A. Stirling, A. Hamza, I. Pápai, *J. Am. Chem. Soc.* **2013**, *135*, 4425.

[10] a) S. Grimme, H. Kruse, L. Goerigk, G. Erker, *Angew. Chem. Int. Ed.* **2010**, *49*, 1402; *Angew. Chem.* **2010**, *122*, 1444; b) B. Schirmer, S. Grimme, *Chem. Commun.* **2010**, *46*, 7942.

[11] a) É. Dorkó, E. Varga, T. Gáti, T. Holczbauer, I. Pápai, H. Mehdi, T. Soós, *Synlett* **2014**, *25*, 1525. For a computational study on other possible side reactions, see: b) L. Zhao, G. Lu, F. Huang, Z-X. Wang, *Dalton Trans.* **2012**, *41*, 4674.

[12] For the geminal B/N FLP 1-[bis(pentafluorophenyl)boryl]-3,5-di-tert-butyl-1*H*-pyrazole, see E. Theuergarten, J. Schlösser, D. Schlüns, M. Freytag, C. G. Daniliuc, P. G. Jones, M. Tamm, *Dalton Trans.* **2012**, *41*, 9101.

[13] For $R_2PCH_2BPh_2$ systems, see: a) F. Bertini, V. Lyaskoyskyy, B. J. J. Timmer, F. J. J. de Kanter, M. Lutz, A. W. Ehlers, J. C. Slootweg, K. Lammertsma, *J. Am. Chem. Soc.* **2012**, *134*, 201; b) E. R. M. Habraken, L. C. Mens, M. Nieger, M. Lutz, A. W. Ehlers, J. C. Slootweg, *Dalton Trans.* **2017**, *46*, 12284.

[14] Gaussian 09, Revision D.01, M. J. Frisch, G. W. Trucks, H. B. Schlegel, G. E. Scuseria, M. A. Robb, J. R. Cheeseman, G. Scalmani, V. Barone, B. Mennucci, G. A. Petersson, H. Nakatsuji, M. Caricato, X. Li, H. P. Hratchian, A. F. Izmaylov, J. Bloino, G. Zheng, J. L. Sonnenberg, M. Hada, M. Ehara, K. Toyota, R. Fukuda, J. Hasegawa, M. Ishida, T. Nakajima, Y. Honda, O. Kitao, H. Nakai, T. Vreven, J. A. Montgomery, Jr., J. E. Peralta, F. Ogliaro, M. Bearpark, J. J. Heyd, E. Brothers, K. N. Kudin, V. N. Staroverov, R. Kobayashi, J. Normand, K. Raghavachari, A. Rendell, J. C. Burant, S. S. Iyengar, J. Tomasi, M. Cossi, N. Rega, J. M. Millam, M. Klene, J. E. Knox, J. B. Cross, V. Bakken, C. Adamo, J. Jaramillo, R. Gomperts, R. E. Stratmann, O. Yazyev, A. J. Austin, R. Cammi, C. Pomelli, J. W. Ochterski, R. L. Martin, K. Morokuma, V. G. Zakrzewski, G. A. Voth, P. Salvador, J. J. Dannenberg, S. Dapprich, A. D. Daniels, Ö. Farkas, J. B. Foresman, J. V. Ortiz, J. Cioslowski, and D. J. Fox, Gaussian, Inc., Wallingford CT, **2009**.

[15] Y. Zhao, D. G. Truhlar, *Theor. Chem. Acc.* **2008**, *120*, 215.

[16] F. Weigend, R. Ahlrichs, *Phys. Chem. Chem. Phys.* **2005**, *7*, 3297.

[17] C. Gonzalez, H. B. Schlegel, *J. Phys. Chem.* **1990**, *94*, 5523.

[18] a) S. Miertuš, E. Scrocco, J. Tomasi, *Chem. Phys.* **1981**, *55*, 117; b) J. L. Pascual-Ahuir, E. Silla, I. Tuñón, *J. Comput. Chem.* **1994**, *15*, 1127; c) V. Barone, M. Cossi, *J. Phys. Chem. A* **1998**, *102*, 1995.

[19] a) C. Fonseca Guerra, J. G. Snijders, G. te Velde, E. J. Baerends, *Theor. Chem. Acc.* **1998**, *99*, 391; b) G. te Velde, F. M. Bickelhaupt, E. J. Baerends, C. Fonseca-Guerra, S. J. A. van Gisbergen, J. G. Snijders, T. Ziegler, *J. Comput. Chem.* **2001**, *22*, 931; c) E. J. Baerends, T. Ziegler, J. Autschbach, D. Bashford, A. Bérces, et al. *ADF2014*, SCM, Theoretical Chemistry, Vrije Universiteit, Amsterdam, The Netherlands, http://www.scm.com.

[20] a) S. H. Vosko, L. Wilk, M. Nusair, *Can. J. Phys.* **1980**, *58*, 1200; b) A. D. Becke, *Phys. Rev. A* **1988**, *38*, 3098; c) J. P. Perdew, *Phys. Rev. B* **1986**, *33*, 8822.

[21] a) S. Grimme, *J. Comput. Chem.* **2006**, *27*, 1787; b) S. Grimme, J. Antony, S. Ehrlich, H. Krieg, *J. Chem. Phys.* **2010**, *132*, 154104.

[22] a) E. van Lenthe, E. J. Baerends, *J. Comput. Chem.* **2003**, *24*, 1142; b) M. Franchini, P. H. T. Philipsen, E. van Lenthe, L. Visscher, *J. Chem. Theory Comput.* **2014**, *10*, 1994.

[23] a) E. van Lenthe, E. J. Baerends, J. G. Snijders, *J. Chem. Phys.* **1993**, *99*, 4597; b) E. van Lenthe, E. J. Baerends, J. G. Snijders, *J. Chem. Phys.* **1994**, *101*, 9783.

[24] Selected examples: a) D. H. Ess, K. N. Houk, *J. Am. Chem. Soc.* **2007**, *129*, 10646; b) D. H. Ess, K. N. Houk, *J. Am. Chem. Soc.* **2008**, *130*, 10187; c) J. M. Medina, J. L. Mackey, N. K. Garg, K. N. Houk, *J. Am. Chem. Soc.* **2014**, *136*, 15798; d) B. J. Levandowski, T. A. Hamlin, F. M. Bickelhaupt, K. N. Houk, *J. Org. Chem.* **2017**, *82*, 8668.

[25] Representative recent examples: a) D. N. Kamber, L. A. Nazarova, Y. Liang, S. A. Lopez, D. M. Patterson, H.-W. Shih, K. N. Houk, J. A. Prescher, *J. Am. Chem. Soc.* **2013**, *135*, 13680; b) Y. Cao, Y. Liang, L. Zhang, S. Osuna, A.-L. M. Hoyt, A. L. Briseno, K. N. Houk, *J. Am. Chem. Soc.* **2014**, *136*, 10743; c) I. Fernández, F. M. Bickelhaupt, F. P. Cossío, *Chem. Eur. J.* **2014**, *20*, 10791; d) F. M. Bickelhaupt, M. Solà, I. Fernández, *Chem. Eur. J.* **2015**, *21*, 5760; e) Y. García-Rodeja, M. Solà, F. M. Bickelhaupt, I. Fernández, *Chem. Eur. J.* **2016**, *22*, 1368; f) Y. García-Rodeja, M. Solà, I. Fernández, *Chem. Eur. J.* **2016**, *22*, 10572; g) D. Yepes, P. Pérez, P. Jaque, I. Fernández, *Org. Chem. Front.* **2017**, *4*, 1390.

[26] a) W.-J. van Zeist, F. M. Bickelhaupt, *Dalton Trans.* **2011**, *40*, 3028, and references therein; b) L. P. Wolters, F. M. Bickelhaupt, *ChemistryOpen* **2013**, *2*, 106; c) A. G. Green, P. Liu, C. A. Merlic, K. N. Houk, *J. Am. Chem. Soc.* **2014**, *136*, 4575; d) I. Fernández, L. P. Wolters, F. M. Bickelhaupt, *J. Comput. Chem.* **2014**, *35*, 2140; e) E. D. Sosa Carrizo, F. M. Bickelhaupt, I. Fernández, *Chem. Eur. J.* **2015**, *21*, 14362; f) Y. García-Rodeja, I. Fernández, *Organometallics* **2017**, *36*, 460.

[27] a) K. Morokuma, *J. Chem. Phys.* **1971**, *55*, 1236; b) T. Ziegler, A. Rauk, *Theor. Chim. Acta* **1977**, *46*, 1.

[28] M. P. Mitoraj, A. Michalak, T. Ziegler, *J. Chem. Theory Comput.* **2009**, *5*, 962.

[29] a) S. Sankararaman, *Pericyclic Reactions—A Textbook: Reactions, Applications and Theory*, Wiley-VCH, Weinheim, **2005**; pp. 326 – 329, and references therein. See also, b) I. Fernández, M. A. Sierra, F. P. Cossío, *J. Org. Chem.* **2007**, *72*, 1488.

[30] a) S. Hünig, H. R. Müller, W. Thier, *Angew. Chem. Int. Ed. Engl.* **1965**, *4*, 271; *Angew. Chem.* **1965**, *77*, 368; b) M. Franck-Neumann, C. Dietrich-Buchecker, *Tetrahedron Lett.* **1980**, *21*, 671; c) E. W. Garbisch, Jr., S. M. Schildcrout, D. B. Patterson, C. M. Sprecher, *J. Am. Chem. Soc.* **1965**, *87*, 2932.

[31] L. Sominsky, E. Rozental, H. Gottlieb, A. Gedanken, S. Hoz, *J. Org. Chem.* **2004**, *69*, 1492.

[32] For a review on dyotropic reactions, see: I. Fernández, F. P. Cossío, M. A. Sierra, *Chem. Rev.* **2009**, *109*, 6687.

[33] a) R. Noyori, T. Okhuma, M. Kitamura, H. Takaya, N. Sayo, H. Kumobayashi, S. Akuragawa, *J. Am. Chem. Soc.* **1987**, *109*, 5856; b) C. A. Sandoval, T. Ohkuma, K. Muñiz, R. Noyori, *J. Am. Chem. Soc.* **2003**, *125*, 13490. See also: c) O. Nieto Faza, I. Fernández, C. Silva López, *Chem. Commun.* **2013**, *49*, 4277.

[34] For other geminal N/B FLP examples, see: a) L. Zhao, H. Li, G. Lu, F. Huang, C. Zhang, Z.-X. Wang, *Dalton Trans.* **2011**, *40*, 1929. See also refs. [11, 12].

[35] A similar concerted H_2 release has been found computationally for completely different (nongeminal) intramolecular FLPs, see: P. Pérez, D. Yepes, P. Jaque, E. Chamorro, L.-R. Domingo, R. S. Rojas, A. Toro-Labbé, *Phys. Chem. Chem. Phys.* **2015**, *17*, 10715. See also reference [11b].

[36] a) J. E. Leffler, *Science* **1953**, *117*, 340; b) G. S. J. Hammond, *J. Am. Chem. Soc.* **1955**, *77*, 334.

[37] a) E. R. Johnson, S. Keinan, P. Mori-Sánchez, J. Contreras-García, A. J. Cohen, W. Yang, *J. Am. Chem. Soc.* **2010**, *132*, 6498; b) J. Contreras-García, E. R. Johnson, S. Keinan, R. Chaudret, J.-P. Piquemal, D. N. Beratan, W. Yang, *J. Chem. Theory Comput.* **2011**, *7*, 625.

[38] I. Fernández, F. M. Bickelhaupt, F. P. Cossío, *Chem. Eur. J.* **2009**, *15*, 13022.

[39] For a perspective on the application of the ASM method on pericyclic reactions, see: a) I. Fernández, *Phys. Chem. Chem. Phys.* **2014**, *16*, 7662. For Diels – Alder reactions, see also: b) I. Fernández, F. M. Bickelhaupt, *Chem. Asian J.* **2016**, *11*, 3297.

Manuscript received: February 20, 2018
Accepted manuscript online: April 14, 2018
Version of record online: May 22, 2018

 © 2018 Wiley-VCH Verlag GmbH & Co. KGaA, Weinheim